Research Article
Innovative Diagnostics, Modelling and Digital Hepatology

JOURNAL
OF HEPATOLOGY

Digital pathology with artificial intelligence analyses provides greater insights into treatment-induced fibrosis regression in NASH

Graphical abstract

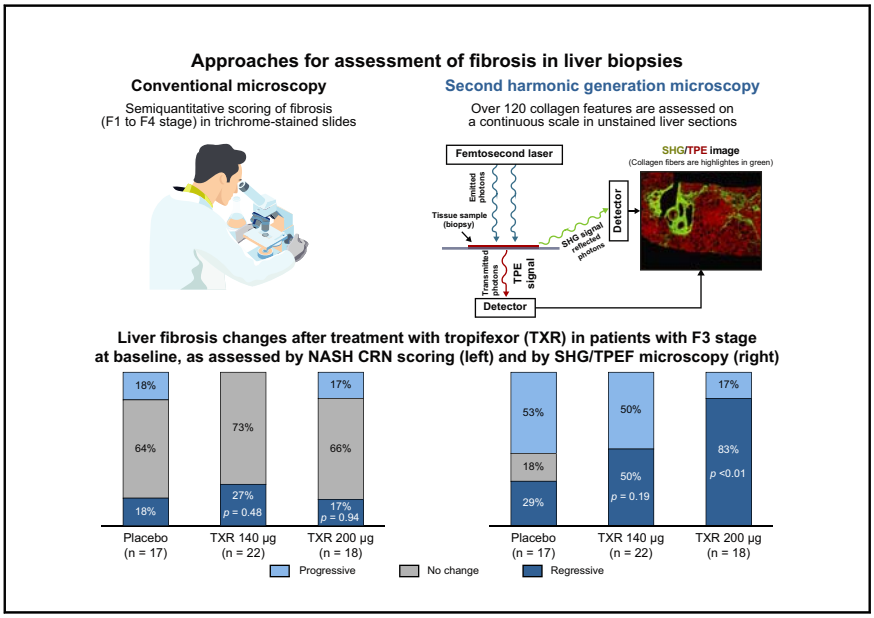

Highlights

- AI revealed antifibrotic effects of TXR, unlike conventional microscopy.
- Spatial correlation between fibrosis and steatosis reduction suggests that anti-metabolic therapies initially drive fibrosis regression in the perisinusoidal regions.
- Regressive changes in septa morphology and collagen fiber parameters observed in patients with F3 fibrosis, who were considered 'unchanged' with conventional scoring.
- Digital pathology provides quantitative details of fibrosis dynamics with novel insights into treatment-induced fibrosis regression in NASH.

Authors

Nikolai V. Naoumov,
Dominique Brees, Juergen Loeffler,
…, Dean Tai, Sophie Lamle,
Arun J. Sanyal

Correspondence

nikolainaoumov@yahoo.com (N.V. Naoumov).

Lay summary

The degree of liver fibrosis (tissue scarring) in non-alcoholic steatohepatitis (NASH) is the main predictor of negative clinical outcomes. Accurate assessment of the quantity and architecture of liver fibrosis is fundamental for patient enrolment in NASH clinical trials and for determining treatment efficacy. Using digital microscopy with artificial intelligence analyses, the present study demonstrates that this novel approach has greater sensitivity in demonstrating treatment-induced reversal of fibrosis in the liver than current systems. Furthermore, additional details are obtained regarding the pathogenesis of NASH disease and the effects of therapy.

https://doi.org/10.1016/j.jhep.2022.06.018
 J. Hepatol. 2022, 77, 1399–1409

Research Article
Innovative Diagnostics, Modelling and Digital Hepatology

JOURNAL OF HEPATOLOGY

Digital pathology with artificial intelligence analyses provides greater insights into treatment-induced fibrosis regression in NASH

Nikolai V. Naoumov[1,*], Dominique Brees[1], Juergen Loeffler[1], Elaine Chng[2], Yayun Ren[2], Patricia Lopez[1], Dean Tai[2], Sophie Lamle[1], Arun J. Sanyal[3]

[1]*Novartis Pharma AG, Basel, Switzerland;* [2]*HistoIndex Pte. Ltd, Singapore;* [3]*Virginia Commonwealth University School of Medicine, Richmond, United States*

Background & Aims: Liver fibrosis is a key prognostic determinant for clinical outcomes in non-alcoholic steatohepatitis (NASH). Current scoring systems have limitations, especially in assessing fibrosis regression. Second harmonic generation/two-photon excitation fluorescence (SHG/TPEF) microscopy with artificial intelligence analyses provides standardized evaluation of NASH features, especially liver fibrosis and collagen fiber quantitation on a continuous scale. This approach was applied to gain in-depth understanding of fibrosis dynamics after treatment with tropifexor (TXR), a non-bile acid farnesoid X receptor agonist in patients participating in the FLIGHT-FXR study (NCT02855164).

Method: Unstained sections from 198 liver biopsies (paired: baseline and end-of-treatment) from 99 patients with NASH (fibrosis stage F2 or F3) who received placebo (n = 34), TXR 140 μg (n = 37), or TXR 200 μg (n = 28) for 48 weeks were examined. Liver fibrosis (qFibrosis®), hepatic fat (qSteatosis®), and ballooned hepatocytes (qBallooning®) were quantitated using SHG/TPEF microscopy. Changes in septa morphology, collagen fiber parameters, and zonal distribution within liver lobules were also quantitatively assessed.

Results: Digital analyses revealed treatment-associated reductions in overall liver fibrosis (qFibrosis®), unlike conventional microscopy, as well as marked regression in perisinusoidal fibrosis in patients who had either F2 or F3 fibrosis at baseline. Concomitant zonal quantitation of fibrosis and steatosis revealed that patients with greater qSteatosis reduction also have the greatest reduction in perisinusoidal fibrosis. Regressive changes in septa morphology and reduction in septa parameters were observed almost exclusively in F3 patients, who were adjudged as 'unchanged' with conventional scoring.

Conclusion: Fibrosis regression following hepatic fat reduction occurs initially in the perisinusoidal regions, around areas of steatosis reduction. Digital pathology provides new insights into treatment-induced fibrosis regression in NASH, which are not captured by current staging systems.

Lay summary: The degree of liver fibrosis (tissue scarring) in non-alcoholic steatohepatitis (NASH) is the main predictor of negative clinical outcomes. Accurate assessment of the quantity and architecture of liver fibrosis is fundamental for patient enrolment in NASH clinical trials and for determining treatment efficacy. Using digital microscopy with artificial intelligence analyses, the present study demonstrates that this novel approach has greater sensitivity in demonstrating treatment-induced reversal of fibrosis in the liver than current systems. Furthermore, additional details are obtained regarding the pathogenesis of NASH disease and the effects of therapy.

Introduction

Non-alcoholic fatty liver disease (NAFLD) is the most common chronic liver disease at present; it affects ~25% of the adult population worldwide.[1,2] NAFLD is caused by metabolic disorders leading to accumulation of various amounts of fat in hepatocytes, while a proportion of patients also develop non-alcoholic steatohepatitis (NASH) with liver injury, inflammation, and often varying degrees of liver fibrosis. The natural course of NAFLD includes 3 consecutive phases: non-alcoholic fatty liver with steatosis alone (with no evidence of injury or inflammation), non-cirrhotic NASH, and NASH with cirrhosis, which are associated with progressively increasing mortality risk and no approved drug therapy at present.[3–5]

In patients with NASH, the degree of liver fibrosis is the principal feature that predicts clinical outcomes.[6–9] Fibrosis deposition is dynamic, resulting from both fibrogenesis and fibrolysis, even during architectural remodeling of the liver and disease progression to cirrhosis.[4,9] Therefore, understanding the drivers and mechanisms of collagen accumulation, as well as fibrosis regression, is critical for improving the management and outcomes of patients with NASH. Assessment of liver histology is the gold standard for correct diagnosis of NASH and is also essential to exclude potential coincident liver diseases.[10–12] Furthermore, semi-quantitative scoring of key NASH features (steatosis, lobular inflammation, hepatocyte ballooning, with or without fibrosis) is key for determining NAFLD activity and fibrosis stage; these are the basis for patients' enrolment in NASH clinical trials. Similarly, for drug approval, these histological features of NASH are the basis for the current primary endpoints in phase II and III NASH trials, as agreed by the regulatory authorities.[3,13] Several histological scoring systems

Keywords: Non-alcoholic Steatohepatitis; Digital Pathology with Artificial Intelligence; Second Harmonic Generation Microscopy; Fibrosis Regression; Perisinusoidal Fibrosis; Farnesoid X Receptor Agonists and NASH Treatment.
Received 24 September 2021; received in revised form 21 May 2022; accepted 10 June 2022; available online 30 June 2022
* Corresponding author. Address: 144 Clonmore Street, London SW18 5HB, United Kingdom; Tel.: +44 7767076948.
E-mail address: nikolainaoumov@yahoo.com (N.V. Naoumov).
https://doi.org/10.1016/j.jhep.2022.06.018

have been developed to grade NAFLD activity and the staging of liver fibrosis.[14–16] These systems were initially developed to score disease progression; however, they were not optimized to score regression or treatment response. Furthermore, they have limitations which are increasingly recognized as providing subjective, categorical descriptions, without capturing details of fibrosis dynamics;[14,17,18] suboptimal quantitation of perisinusoidal fibrosis;[18] substantial intra- and inter-observer variations;[14,17,19,20] as well as a limited dynamic range in demonstrating fibrosis regression within the broad categories of NASH with advanced fibrosis (F3) or NASH cirrhosis (F4).[18,21] These inherent limitations hamper progress in the understanding of NASH pathogenesis and create challenges for drug development in NASH with respect to the definition of trial endpoints, patient enrolment, and accurate and reproducible assessment of treatment response.

The use of second harmonic generation/two-photon excitation fluorescence (SHG/TPEF) microscopy allows for the identification of individual collagen fibers and fibrosis localization in 2D and 3D formats with precise quantification of physical features, *e.g.* number, length, width and cross-linkages in unstained tissue sections.[22,23] SHG/TPEG has provided accurate and reproducible fibrosis quantification in preclinical and clinical liver specimens,[24] and has been successfully applied to quantify collagen deposition in biopsies from pediatric and adult patents with NAFLD.[25–27] Recognizing these potential advantages of digital pathology with artificial intelligence (AI), paired liver biopsies (baseline [BL] and end-of-treatment [EOT]) from patients with non-cirrhotic NASH who participated in the FLIGHT-FXR clinical trial (NCT02855164) were analyzed. The aim of this exploratory *post hoc* analysis was to gain an in-depth understanding of liver fibrosis regression and its relationship with steatosis and hepatocyte ballooning changes after treatment with tropifexor (TXR), a selective non-bile acid farnesoid X receptor agonist.[28]

Patients and methods

Clinical study details

The clinical details and laboratory data for the present study were generated in the FLIGHT-FXR clinical trial, which has been presented previously.[28] In brief, FLIGHT-FXR is a phase II randomized, double-blind, placebo-controlled, dose-finding study with an adaptive design consisting of 3 sequential Parts (A, B, and C) assessing the safety and efficacy of TXR in patients with NASH. TXR has shown high potency of target engagement and antifibrotic effects in preclinical studies.[29,30] The FLIGHT-FXR trial included adult male and female patients with elevated alanine aminotransferase (ALT; males ≥43 IU/L; females ≥28 IU/L) and hepatic fat fraction (HFF) ≥10% at screening (as assessed by MRI-proton density fat fraction). Parts A and B had a 12-week duration and evaluated TXR doses of 10–90 μg.

Part C included patients with biopsy-proven NASH and fibrosis stage F2 or F3, based on the NASH clinical research network (CRN) scoring system[14] and evaluated TXR doses of 140 and 200 μg *vs.* placebo (1:1:1) for 48 weeks, with a planned interim analysis at Week 12. The study primary endpoints included safety, tolerability, and changes in ALT and HFF from BL to Week 12.

Conventional liver histology assessment

Patients enrolled in Part C underwent a liver biopsy during the screening period (within 6 months or less prior to randomization) and at EOT (Week 48). Prior to randomization, liver biopsies were evaluated by the central histopathologist to confirm eligibility.

Treatment-associated changes in liver histology (BL to EOT) were key secondary endpoints in Part C of the FLIGHT-FXR trial according to the regulatory recommended endpoints.[3,13] The histological assessment involved paired biopsy evaluation, *i.e.* the BL and Week 48 biopsies for each patient were read together, at the same time by the central histopathologist, who was blinded to subject identification, type of treatment, and timepoint. The collagen proportionate area (CPA) was determined, as described previously,[31] and expressed as percentage collagen area of the total liver tissue area.

SHG/TPEF microscopy and AI analyses

Unstained, formalin-fixed sections from 198 paired liver biopsies (BL and EOT) from 99 patients with NASH (fibrosis stage F2 [n = 42], or F3 [n = 57]) who received placebo (n = 34), TXR 140 μg (n = 37), or TXR 200 μg (n = 28) for 48 weeks were examined using SHG/TPEF microscopy with computer-assisted analyses. The liver sections were de-paraffinized and tissue scanning was performed on Genesis®200 (a fully automated, stain-free multi-photon fluorescence imaging microscope) and analyzed using AI-based algorithms (HistoIndex Pte. Ltd), as described previously.[26,27] Samples were laser-excited at 780 nm, SHG signals were recorded at 390 nm, and TPEF signals were recorded at 550 nm. Images were acquired at 20X magnification with a 512 ×512 pixels resolution; each image tile had a dimension of 200 ×200 μm. Multiple adjacent image tiles were captured to encompass the whole tissue areas in each slide. The liver biopsies from FLIGHT-FXR provided large specimens for quantitation analyses, the AI computer-assisted measurement of all scanned biopsies showed a median length of 35 mm (9–87 mm), with a median number of portal tracts of 40 (6–119).

The SHG/TPEF examination and analyses were performed blinded to type of treatment, timepoint, central pathologist's scoring, and without knowledge of any results from clinical trial investigations. The algorithm for digital assessment of lobular inflammation is currently under development to improve previously published outputs,[27] so inflammation was not included in the present analyses.

Key parameters for quantitation of liver fibrosis, steatosis, and hepatocyte ballooning

qFibrosis® is the overall output from assessment of fibrosis in the liver specimen comprising the quantitative readouts from 128 fibrosis parameters on a linear scale.[27] It quantifies the fibrosis overall, as well as fibrous depositions in different areas of the liver lobule (portal, periportal, transitional, pericentral), as well as specific morphological features of collagen fibers, such as fiber length, width, and area. The periportal and pericentral areas are set at 100 μm from the portal tract and central vein, respectively, and the region in between marks the transitional area. The 100 μm measure is an approximation, based on a tenth of the average distance between the portal tract and central vein in a normal liver. qFibrosis® calculation is based on normalized collagen parameters expressed as the number of units per mm^2

and provides unbiased, highly reproducible assessment of the severity of liver fibrosis.[27,32] Taking into account that NASH treatment with compounds which markedly reduce liver fat content can alter the area used for fibrosis quantitation, especially when comparing pre- and post-treatment fibrosis, a steatosis correction was applied when assessing fibrosis dynamics within the liver lobule. For this purpose, the steatosis area, as determined by SHG/TPEF microscopy, was subtracted from the total liver area to ensure that the denominator is the same for quantitation of fibrosis in different zones of the liver lobule at BL and after 48 weeks of treatment with TXR.

SHG/TPEF microscopy with AI analyses was also used to quantify the liver fat content (qSteatosis®) in the entire specimen.[27] This also enabled the determination of different sizes and numbers of fat vacuoles in hepatocytes and their changes following TXR treatment. Furthermore, TXR treatment-induced changes of collagen fibers in relation to steatosis changes were evaluated by simultaneous measurement of fibrosis and hepatic fat in selected areas within 14 μm around the fat vacuoles in the liver lobule.

The number of ballooned hepatocytes in the entire liver specimen, along with additional parameters, such as the area of ballooned hepatocytes, density of ballooned cells, and collagen fibers around ballooned cells, was also quantitated. All parameters were normalized per tissue area (unit tissue area, 1 μm^2). A continuous qBallooning value is generated based on these parameters, using an algorithm trained by 9 internationally recognized liver pathologists.[33] To convert the composite qBallooning readouts into qBallooning grades, cut-off values were generated by correlating the continuous qBallooning values from the FLIGHT-FXR cohort with the central reader's ballooning grading, and the respective qBallooning grades (0,1,2) were determined based on these cut-off values. Details on the conversion of continuous qBallooning values to a semi-quantitative qBallooning grade has been reported previously.[27]

Statistical analyses

All available results of participants who had a BL and EOT assessment were included in statistical analyses. Missing data were not imputed. Correlations were analyzed using a Spearman's rank correlation coefficient. The change of qFibrosis from BL was analyzed using analysis of covariance adjusted by the BL value. *P* values are for the comparisons *vs.* placebo. All *p* values are descriptive and unadjusted for multiple testing. The fibrosis dynamics (BL to EOT) between the TXR and placebo treatment arms were compared using **P**rogressive/**N**o Change/**R**egressive (P/N/R) analysis. The number of cases in each subgroup was divided by the total number of patients in each arm to obtain the percentages shown. A Chi-square test was applied to the P/N/R analysis. In the colocalization analysis, a Wilcoxon signed rank test was used.

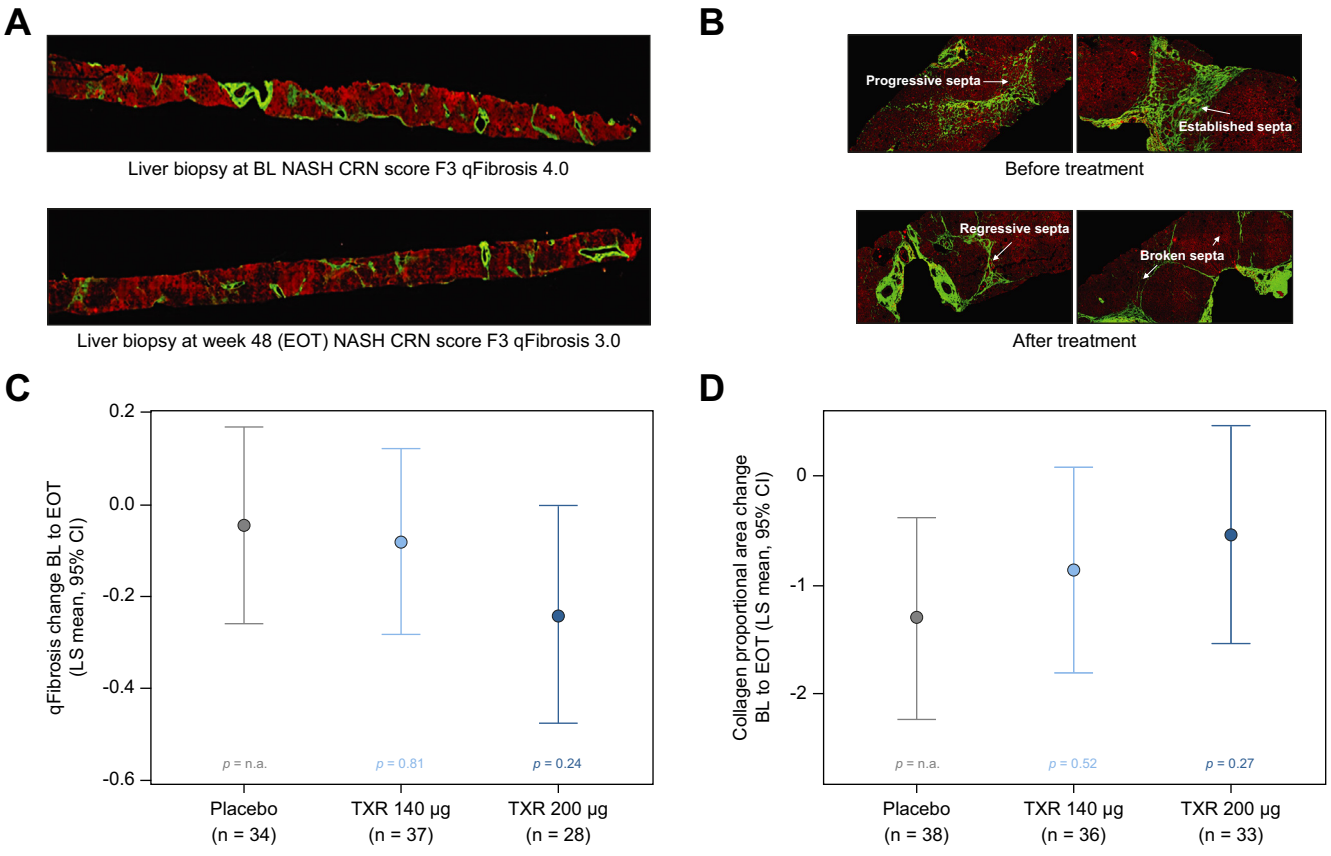

Fig. 1. Digital assessment of liver fibrosis demonstrates fibrosis reduction in patients receiving TXR. (A) A representative case with BL and EOT biopsies as visualized by SHG/TPEF microscopy. (B) Morphological patterns of fibrous septa before and after treatment. (C) Changes of qFibrosis (BL to EOT) in the 3 treatment groups. (D) Changes in CPA (BL to EOT) in the 3 treatment groups. *p* values for difference to placebo are from ANCOVA adjusted by baseline value, no multiplicity correction. ANCOVA, analysis of covariance; BL, baseline; CPA, collagen proportionate area; CRN, Clinical Research Network; EOT, end-of-treatment; LS, least squares; n, number of patients; SHG/TPEF, second harmonic generation/two-photon excitation fluorescence microscopy; TXR, tropifexor.

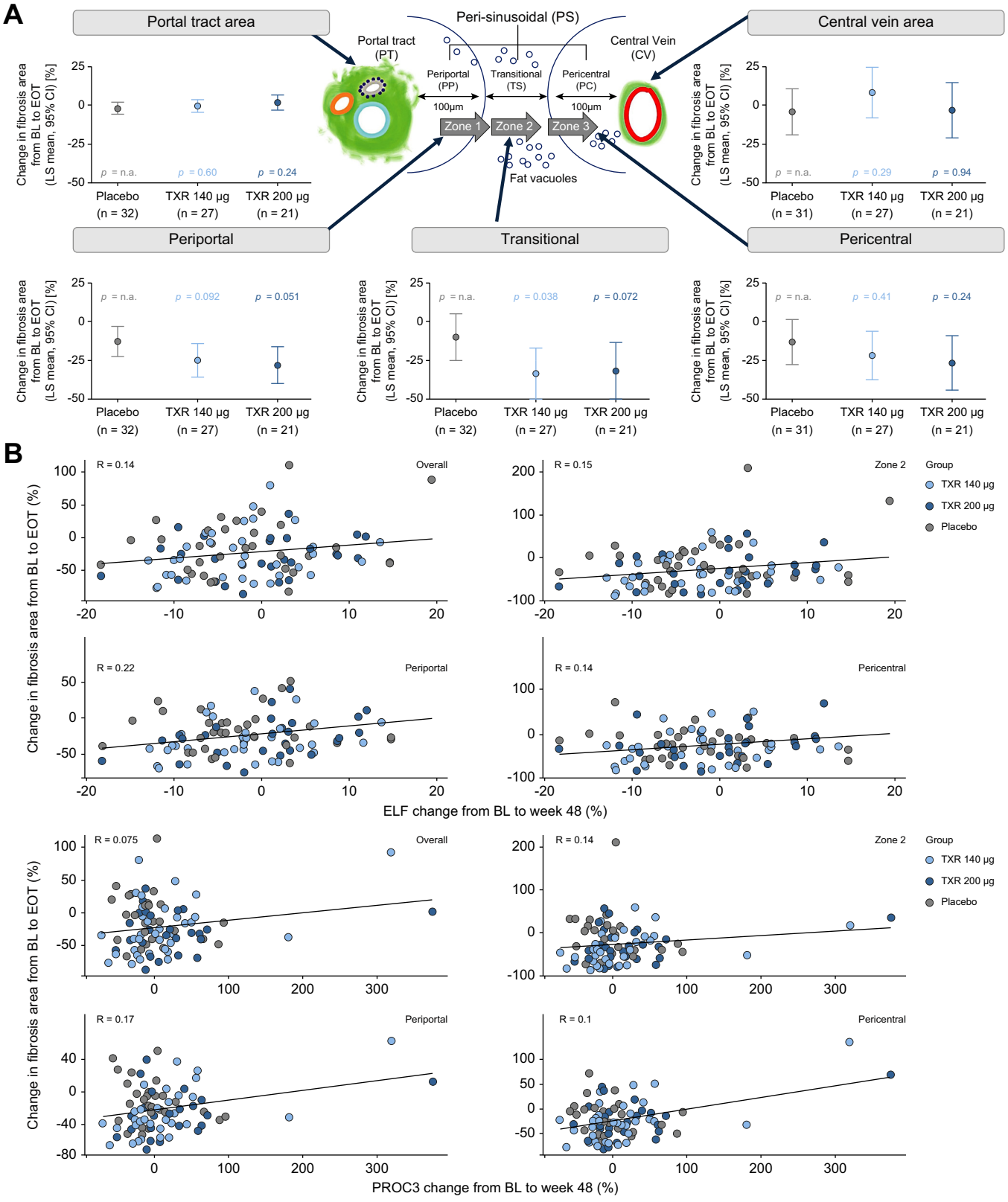

Fig. 2. Treatment-induced fibrosis regression in the perisinusoidal area and correlation with serum fibrosis markers. (A) Zonal fibrosis quantitation, as a percentage change of fibrosis area from BL to EOT, reveals marked fibrosis reduction in the perisinusoidal area. *P* values for difference to placebo are from ANCOVA adjusted by baseline value, no multiplicity correction. (B) Correlations between the percentage change of fibrosis area (overall and in specific regions), with ELF and Pro-C3 changes from BL to EOT. Correlations were analyzed using a Spearman's rank correlation coefficient. ANCOVA, analysis of covariance; BL, baseline; ELF, Enhanced Liver Fibrosis; EOT, end-of-treatment; LS, least squares; n, number of patients; PRO-C3, precisely cleaved N-terminal propeptide of type III collagen; TXR, tropifexor.

Results

Digital quantitation of treatment-induced changes of liver fibrosis

qFibrosis® measurement in pre- and post-treatment biopsies revealed fibrosis reduction after 48-week treatment with TXR (Fig. 1A). In BL biopsies there were progressive and established septa which are wide, with loose connective tissue, including inflammatory cells and invading adjacent parenchyma, as described previously.[34] Septa morphology changed following treatment as they became thin and compact with sharp borders from the surrounding liver parenchyma (regressive septa) or broken (Fig. 1B). The absolute change of qFibrosis® from BL to EOT in the 3 study groups showed notable, but non-significant (p = 0.24), fibrosis reduction with TXR 200 μg compared with placebo (Fig. 1C). Liver fibrosis changes (BL to EOT) were also analyzed using CPA measurement (Fig. 1D). There was a

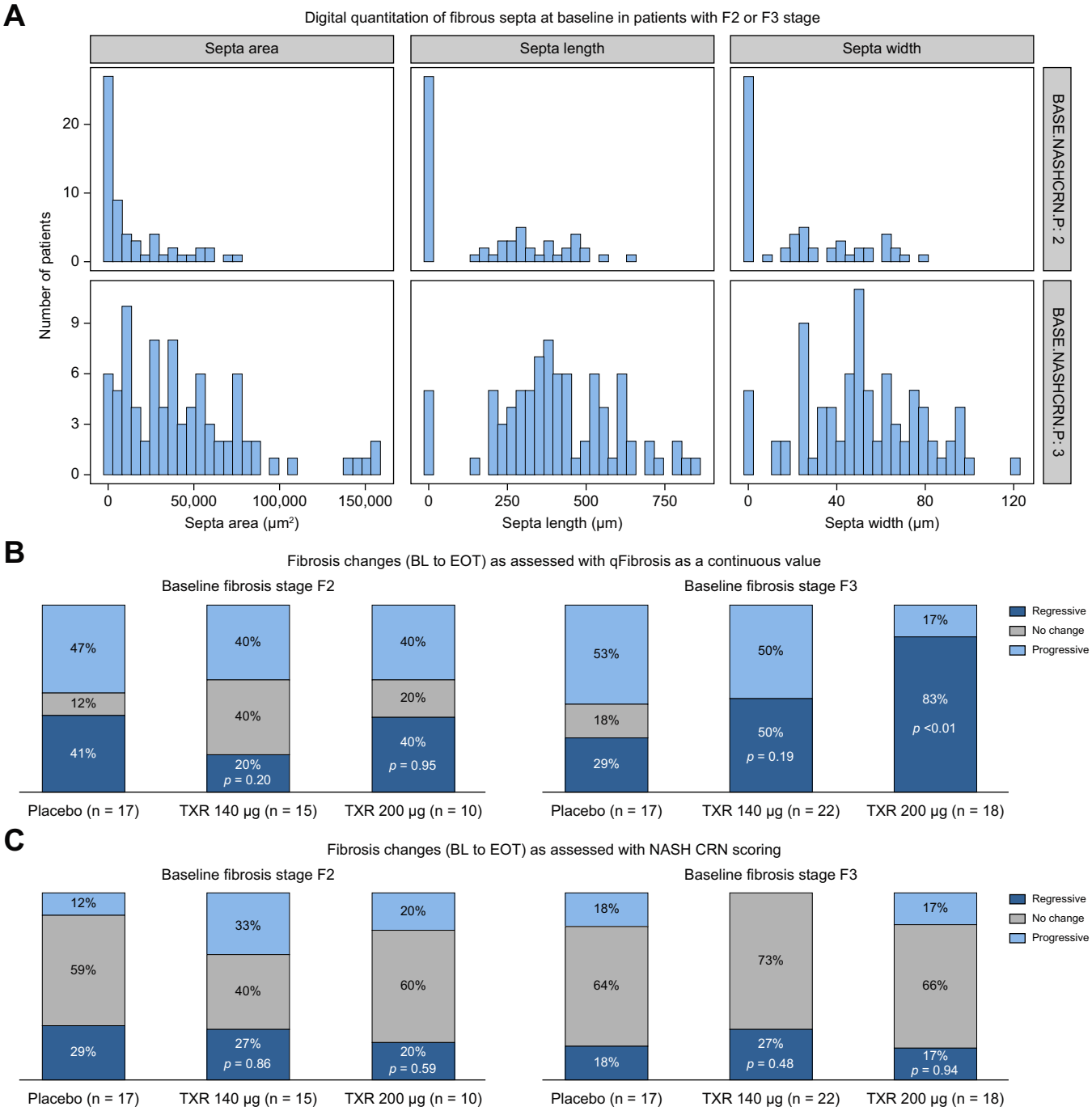

Fig. 3. Fibrosis dynamics in the subgroups of patients with F2 or F3 fibrosis stage at BL, as determined by the central pathologist's score. (A) Digital quantitation of septa area, length, and width at BL. (B) P/N/R analysis of fibrosis changes from BL to EOT, based on qFibrosis assessment as a continuous value. (Progressive–increase by ≥1 standard error of mean; Regressive–decrease by ≥1 standard error of mean). (C) P/N/R analysis of fibrosis changes from BL to EOT, based on the NASH CRN score, as determined by the central pathologist (Progressive–increase by ≥1 fibrosis stage; Regressive–decrease by ≥1 fibrosis stage). *P* values are obtained using a Chi-square test. BL, baseline; EOT, end-of-treatment; CRN, Clinical Research Network; NASH, non-alcoholic steatohepatitis; P/N/R, Progressive/No-change/Regressive; TXR, tropifexor.

moderate correlation (R = 0.4901) between fibrosis assessment by qFibrosis and CPA in baseline liver biopsies from all patients (Fig. S1).

Regression in perisinusoidal fibrosis

The percentage of fibrosis area was also determined in 5 separate regions: the portal tract, periportal (the area within 100 μm around the portal tract), transitional (zone 2), pericentral, and central vein areas (Fig. 2A). The combination of periportal, transitional, and pericentral areas represents the perisinusoidal area with zone 2 being the largest component. Zonal analysis of fibrosis dynamics revealed that 48-week treatment with TXR leads to fibrosis reduction in the perisinusoidal area while there were no changes in fibrosis in the portal tract and central vein areas. Fibrosis reduction was greater in the treatment groups than with placebo, especially in the transitional and periportal areas (Fig. 2A).

The changes in fibrosis (as determined by the percentage change in fibrosis area [overall and in specific regions]), before and after TXR treatment, were correlated with changes in serum fibrosis markers: enhanced liver fibrosis (ELF) and precisely cleaved N-terminal propeptide of type III collagen (PRO-C3) (Fig. 2B). Weak positive correlations were found and overall, serum fibrosis markers did not reflect regression in liver fibrosis as detected by AI digital pathology.

Digital quantitation of septa parameters in patients with F2 and F3 fibrosis stage, as determined by conventional scoring

The analysis of septa parameters showed marked differences, as expected, between the subgroups of patients with fibrosis stage 2 (F2) or 3 (F3) according to CRN scoring of the BL biopsy. In the F3 subgroup, digital quantitation of septa parameters showed high values for septa area, length, and width in almost all cases, while in patients with F2 stage the septa readouts were negative or had low values (Fig. 3A). P/N/R analysis of post-treatment qFibrosis dynamics in F2 patients showed a similar proportion of cases with progressive or regressive changes between the 3 treatment groups when assessed by digital quantitation or by CRN scoring. However, the digital approach markedly reduced the 'no change' subset, especially in the placebo and TXR 200 μg groups (Fig. 3B,C).

In patients with F3 stage, digital quantitation demonstrated a treatment-induced qFibrosis reduction in 50% (11/22) of patients in the TXR 140 μg group and 83% (15/18) with TXR 200 μg *vs.* only 29% (5/17) with placebo (Fig. 3B). Importantly, the proportion of F3 patients with regressive fibrosis changes, as detected by digital quantitation, was greater than with conventional CRN scoring, which showed only 18% (3/17), 27% (6/22), and 17% (3/18) for placebo, TXR 140 μg, and TXR 200 μg, respectively (Fig. 3B,C). The difference was almost exclusively due to the subgroup of F3 patients deemed to have an 'unchanged' ordinal stage, *i.e.* the largest subsets: 66% (12/18) and 73% (16/22) of cases (Fig. 3C). Ten of 11 cases with treatment-induced regressive fibrosis changes, based on digital quantitation, belonged to the 'unchanged' F3 subgroup according to conventional scoring. Furthermore, in patients with F3 fibrosis at BL, additional analyses of treatment-induced changes in septa parameters demonstrated larger reductions of septa area, length, and width in those receiving TXR 200 μg compared with those receiving placebo; however, the difference was not significant (Fig. S2).

Individual, treatment-induced changes in perisinusoidal fibrosis and septa parameters

Individual changes in liver fibrosis parameters were further analyzed (septa parameters and % fibrosis area in zones 2 and 3) between BL and EOT using a waterfall chart (Fig. 4). This analysis confirmed that a larger proportion of patients treated with TXR 200 μg have fibrosis regression compared with placebo, especially notable for patients with F3 fibrosis (light blue bars). The waterfall chart also illustrates that fibrosis regression in septa parameters was present almost exclusively in F3 patients who received TXR, while reduction in perisinusoidal fibrosis (zones 2 and 3) occurred in a greater proportion of patients due to the fact that perisinusoidal fibrosis regression was observed in patients with either F2 or F3 stage at BL.

Colocalization analysis of treatment-induced changes in steatosis and fibrosis within the liver lobule

Digital quantitation of hepatic fat (qSteatosis®) in BL and EOT liver biopsies showed a dose-dependent reduction in patients receiving TXR compared with placebo. The mean changes were: placebo, −0.25; TXR 140 μg, −0.6 (p = 0.047), and TXR 200 μg, −0.95 (p <0.001). The number and the size of fat vacuoles (FVs) within hepatocytes was also quantitated. This method allows for the precise measurement of FVs with a diameter >7 μm, *i.e.* the macrovesicular steatosis that is predominant in NAFLD. In agreement with the dose-dependent reduction of liver fat content after TXR treatment, there were marked changes in the FVs, for example, TXR 200 μg reduced the number of FVs with a 10 μm diameter from 20/μm^2 (at BL) to 13/μm^2 (at EOT) and FVs with a diameter of 20 μm from 10/μm^2 to 5/μm^2 (Fig. 5A). Overall, TXR treatment reduced both the size and the number of FVs per μm^2 of liver area. The relationship between treatment-induced steatosis changes and fibrosis dynamics in the perisinusoidal area was further analyzed by colocalization analysis and simultaneous quantitation of qSteatosis and qFibrosis in selected areas within 14 μm around clusters of FVs (Fig. S3). Patients with unchanged or increased qSteatosis showed only a mild reduction of nearby fibrosis and there was a 58% increase of zone 3 fibrosis in the placebo group (Fig. 5B). In contrast, patients with reduced qSteatosis showed marked fibrosis reduction by 70–80% across the perisinusoidal area (zones 1, 2, and 3; Fig. 5C).

Digital quantitation of hepatocyte ballooning and colocalization analysis of treatment-induced changes in ballooned hepatocytes and fibrosis

To investigate the relationship between treatment-induced changes in ballooned hepatocytes and fibrosis dynamics, colocalization analysis was performed where the characteristics of collagen fibers located within 14 μm around ballooned hepatocytes, *i.e.* fibers in the immediate vicinity of ballooned hepatocytes and clearly separated from other collagen fibers, were determined (Fig. 6A). The analysis of the total number of ballooned hepatocytes (normalized per tissue area) in BL and EOT biopsies demonstrates a shift in the distribution pattern in all 3 study groups: at the EOT, there was an increased number of patients with single ballooned cells along with unchanged or decreased number of cases with large numbers or clusters of ballooned hepatocytes, but these changes were not significant (Fig. 6B). The patients receiving TXR 200 μg showed no change or a decrease in hepatocyte ballooning area between BL and EOT, in contrast to those receiving placebo or TXR 140 μg (Fig. 6C). The colocalization analysis revealed that the decrease of hepatocyte

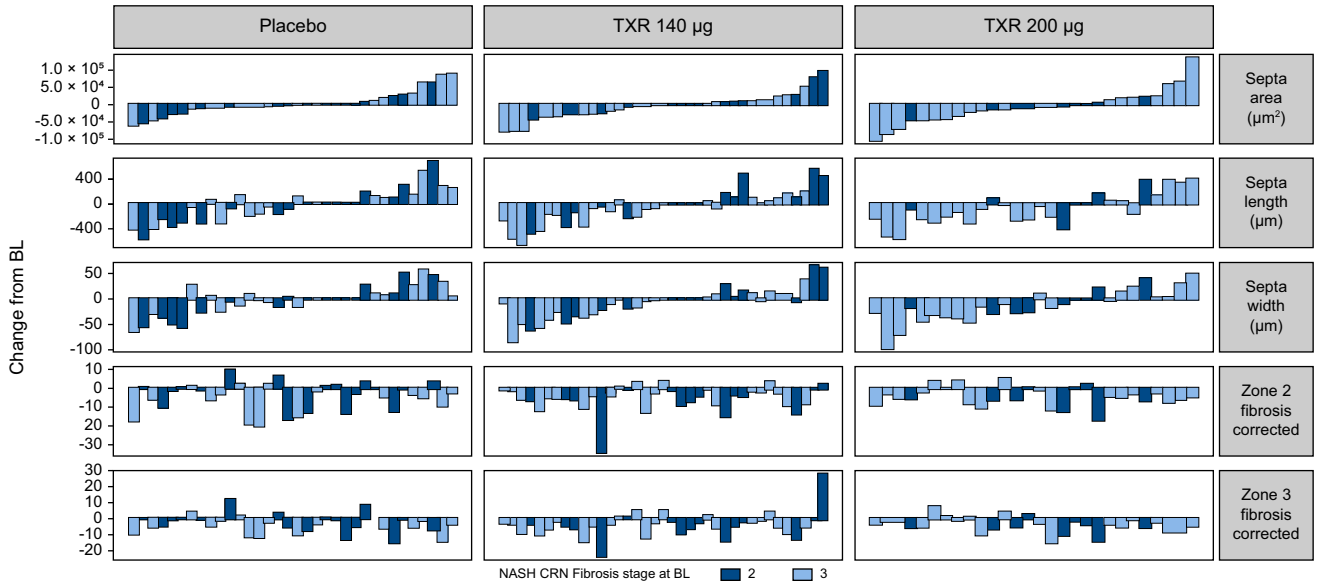

Fig. 4. Waterfall diagram of individual changes (BL to EOT) of septa parameters and perisinusoidal fibrosis. All patients were ordered on the x-axis by the septa area changes. BL, baseline; CRN, Clinical Research Network; EOT, end-of-treatment; TXR, tropifexor.

ballooning, both in the placebo and TXR groups, was associated with a reduction in collagen fibers in the same area (Fig. 6D, right panel).

Discussion

In the present study, the use of digital pathology with SHG/TPEF-derived results reveals 2 novel aspects in NASH: firstly, it provides a new understanding of treatment-induced fibrosis regression starting with marked reduction in perisinusoidal fibrosis in response to decreased fat and lipotoxic drivers in hepatocytes that subsequently extends to portal fibrosis; secondly, it demonstrates the advantages of AI digital pathology by revealing anti-fibrotic effects of TXR which were not captured by the NASH CRN scoring system and conventional microscopy. All

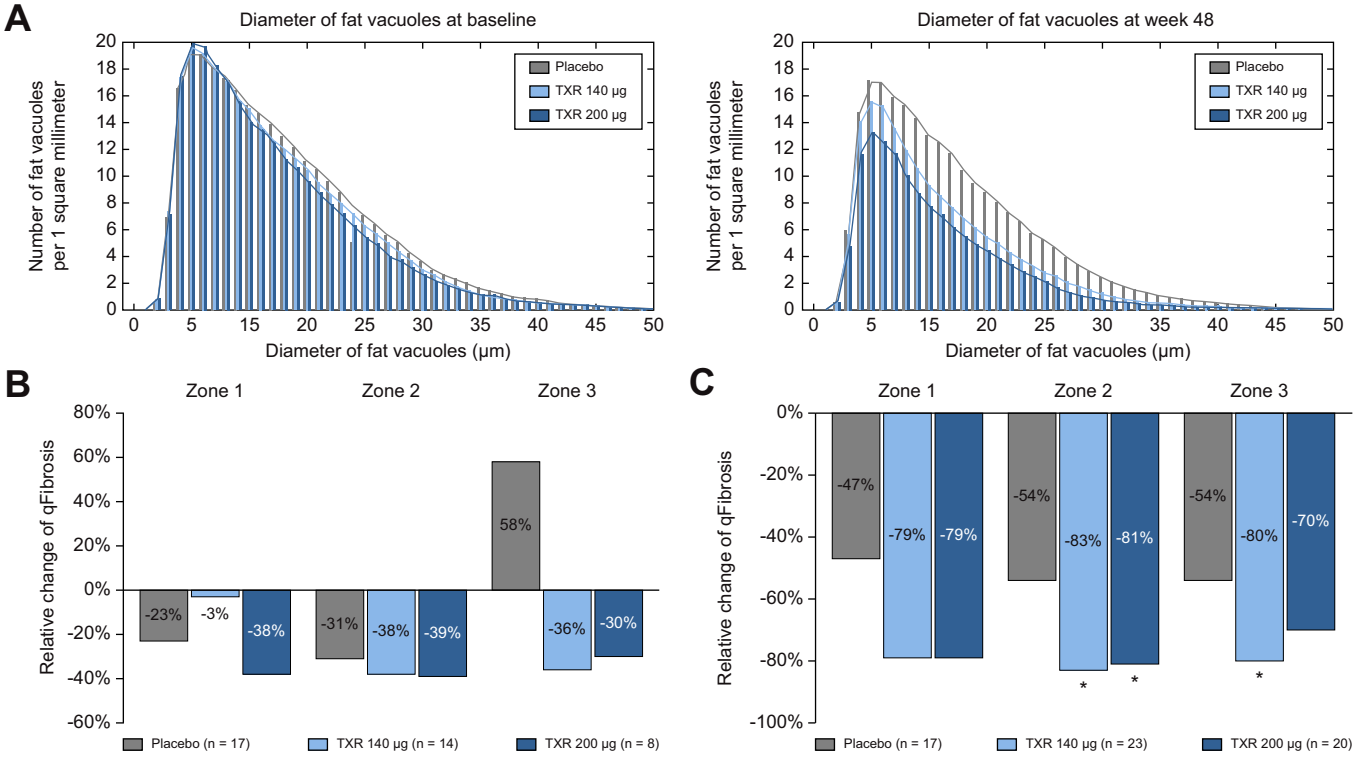

Fig. 5. Quantitation of FVs and colocalization of steatosis and fibrosis changes within the liver lobule. (A) Treatment-induced changes in the number and size of FVs in hepatocytes. (B) Changes in qFibrosis in patients with 'unchanged' or 'increased' qSteatosis (n = 39). (C) Changes in qFibrosis in patients with 'reduced' qSteatosis (n = 60). *p <0.05 compared with placebo, using a Wilcoxon test. FV, fat vacuole; TXR, tropifexor.

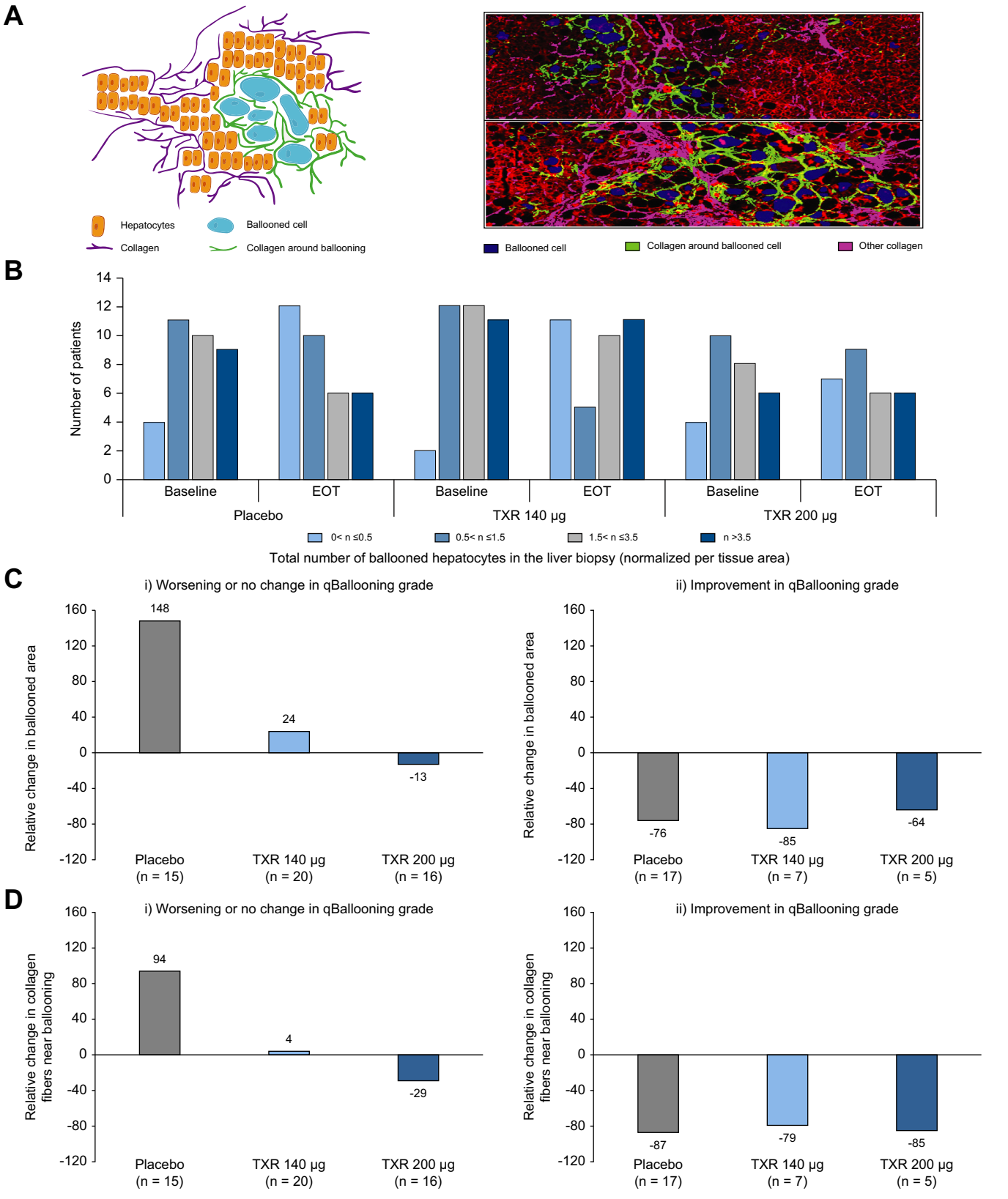

Fig. 6. Digital quantitation of hepatocyte ballooning and colocalization analysis of ballooned hepatocyte and nearby collagen fibers. (A) Colocalization of ballooned hepatocytes and collagen fibers within liver lobule. The characteristics of collagen fibers within 14 µm around ballooned cells were determined. (B) Changes in the distribution of patients according to the total number of ballooned hepatocytes in the liver specimen (normalized per tissue area) at BL and at EOT in the 3 study groups. At the EOT, the number of patients with single ballooned cells increased, while those with large numbers of ballooned hepatocytes decreased or were stable, but these changes were not significant, using a Wilcoxon test. (C and D) Treatment-induced changes of ballooned hepatocytes and nearby collagen fibers. Patients were divided into 2 subsets depending on the qBallooning grade changes from BL to EOT: i) those who had 'worsening' (defined as ≥1 qBallooning grade increase) or 'no change,' and ii) those who had 'improvement' (defined as ≥1 qBallooning grade decrease) in qBallooning grade. (C) Relative change in ballooned area in the 3 study groups. (D) Relative change in collagen fibers near ballooned hepatocytes in the 3 study groups. BL, baseline; EOT, end-of-treatment; TXR, tropifexor.

scoring systems are based on histological changes in untreated individuals, but they do not account well for changes after successful therapy.[35] CRN staging implies that fibrosis progresses from an initial chicken-wire pattern in the perisinusoidal areas (F1), to perisinusoidal plus portal fibrosis (F2), to bridging fibrosis (F3) with fibrosis regression assumed to follow the sequential steps in reverse order.[14,15,18,21] In contrast, the present study reveals marked fibrosis regression in the perisinusoidal areas, in biopsies with F2 or F3 stage, which was more common than the reduction in septa parameters.

A spatial correlation between qFibrosis and qSteatosis reduction in the perisinusoidal regions was also observed following TXR treatment. Similar spatial correlation between steatosis and perisinusoidal fibrosis reduction was observed following treatment with the thyroid-hormone receptor β1 agonist resmetirom,[36] which is likely to be a general mechanism of action for anti-metabolic therapies in NASH, by reducing lipid load and lipotoxicity in hepatocytes where they drive fibrosis regression initially in the perisinusoidal areas.

The use of AI digital pathology also expands the current knowledge of NASH pathobiology by revealing fibrosis regression in patients who were deemed 'unchanged' F3 stage before and after TXR treatment based on CRN scoring. Decreases of multiple septa parameters, as well as regressive changes in septa morphology, were observed in the majority of patients with F3 fibrosis at BL. Hepatic fibrogenesis and collagen turnover are higher in patients with more advanced stages of NASH,[37] which would explain the greater antifibrotic effects of TXR treatment in patients with BL F3 stage *vs.* those with F2. This suggests that SHG/TPEF microscopy will also be highly informative for longitudinal studies or clinical trials involving patients with NASH cirrhosis (F4) who have a wide range of collagen deposition in the liver by providing a quantitative understanding of fibrosis dynamics within the F4 stage and accurately determining treatment-induced fibrosis regression in this important group. Not surprisingly, the details of fibrosis regression, as revealed by digital quantitation, showed only weak correlations with serum makers, ELF and PRO-C3, as the latter were only shown to be informative in combination with other markers or imaging, and mainly in advanced stages of liver fibrosis.[38,39]

The current study highlights the potential benefits of SHG/TPEF with stain-free evaluation of liver biopsies, in parallel with conventional microscopy, by being more sensitive to change within the timeframes of typical phase II and III trials of NASH. An increasing number of studies have utilized SHG/TPEF microscopy to assess fibrosis changes in hepatitis B and NAFLD.[24,27,40–42] Several other digital methodologies have been developed, requiring stained slides, which mostly provide quantitation of predefined NASH features with supervised and/or semi-supervised machine-learning models.[43–48] Collectively, these studies emphasize the innovation and qualities that AI digital pathology brings to investigations of liver diseases, particularly NASH. Indeed, AI digital pathology is expected to be integrated into the workflow of diagnostic and research histopathology in-line with the general trend toward the increasing use of AI in medicine.[42,49–52]

The present study has certain limitations. In particular, the short treatment duration of 48 weeks, with a relatively small number of patients per group have likely reduced the magnitude of treatment-induced differences between TXR and placebo. Future investigations with AI digital pathology involving different mono- and combination treatment regimens will improve the understanding of treatment efficacy and impact of different mechanisms of action in NASH therapy. The clinical relevance of qFibrosis changes, along with digital readouts of specific fibrosis parameters, will need to be established in longitudinal studies with liver-related clinical outcomes. The wider use of AI digital pathology in NASH trials, together with conventional assessments of liver histology, will standardize the quantitative assessment of treatment response, as well as providing valuable additional details, as shown in this study. Digital parameters are currently used as secondary or exploratory endpoints in early phase II trials and the accumulating evidence will enhance all stakeholders' confidence in the benefits of AI digital pathology in NASH drug development. Despite the well-recognized limitations of conventional scoring systems, at present the primary endpoints accepted for phase III trials and accelerated approval are based on the traditional scoring of NASH histology.[3,13] Preliminary data from longitudinal studies indicate that AI digital readouts of liver biopsies can predict hard-endpoints and clinical outcomes in NASH.[41,47] With further validation of AI digital methodologies, with respect to variability in assessing NASH features, reproducibility between centers, magnitude of changes that translate into clinical benefit, ability to predict hard clinical outcomes *etc*., it is expected that AI digital pathology will become the new gold standard for quantitative assessment of liver histology in the not too distant future.

Abbreviations

AI, artificial intelligence; ALT, alanine aminotransferase; BL, baseline; PRO-C3, precisely cleaved N-terminal propeptide of type III collagen; CPA, collagen proportionate area; EOT, end-of-treatment; FV, fat vacuoles; NAFLD, non-alcoholic fatty liver disease; NAS, NAFLD activity score; NASH CRN, NASH Clinical Research Network; NASH, non-alcoholic steatohepatitis; P/N/R, Progressive/No change/Regressive; SHG/TPEF, second harmonic generation/two-photon excitation fluorescence microscopy; TXR, tropifexor.

Financial support

This study was funded by Novartis Global Drug Development, Basel, Switzerland.

Conflict of interest

N.V. Naoumov: Previously employee, Novartis; current: Advisor, HistoIndex, Hepion, InSphero; D. Brees, J. Loeffler, P. Lopez: Employee, Novartis. E. Chng, Y. Ren, D. Tai: Employee, Histoindex. S. Lamle: Previously employee, Novartis; current: Employee, Philip Morris International. A. J. Sanyal: Stockholder: Sanyal Bio, Durect, Genfit, Tiziana, Inversago, Exhalenz; Collaborations: Novartis, Gilead, Intercept, Bristol Myers Squibb, Novo Nordisk, Eli Lilly, Pfizer, Merck, Boehringer Ingelhiem, Hanmi; Advisory Board: NGM Bio, Sequana; Consultant: Intercept, 89Bio, Merck, Pfizer, Genenetech, Gilead, Amgen, Regeneron, Alnylam, Novo Nordisk, Eli Lilly, Siemens, Surrozen, Tern, Poxel, NorthSea, Lipocine, Histoindex, Path AI, Novartis, Astra Zeneca.

Please refer to the accompanying ICMJE disclosure forms for further details.

Authors' contributions

Conceptualization and study design: NVN, DB, DT, SL, AJS; Second Harmonic Generation microscopy: EC, YR, DT; Data collection and analyses: JL, EC, YR, PL, SL, NVN, DB, AJS; Drafting of

manuscript: NVN, DB; All authors contributed to the discussions and interpretation of study results; All authors contributed to the manuscript preparation and approved the final version of the article.

Data availability statement

The data that support the findings of this study are included within the article and its supplementary materials. Data can be available for collaborative investigations upon request with an appropriate institutional collaboration agreement.

Acknowledgment

The authors thank the patients who participated in this study, as well as the investigators and the study coordinators. The authors acknowledge the contribution of Gideon Ho (Histoindex) for helpful discussions of the results and in manuscript preparation. The input of Jogindersingh Paneysar and Lakshya Untwal (Novartis Healthcare Pvt. Ltd.) for the artwork, formatting, and editing of the manuscript is gratefully acknowledged.

Supplementary data

Supplementary data to this article can be found online at https://doi.org/10.1016/j.jhep.2022.06.018.

References

Author names in bold designate shared co-first authorship

[1] Sanyal AJ. Past, present and future perspectives in nonalcoholic fatty liver disease. Nat Rev Gastroenterol Hepatol 2019;16(6):377–386.
[2] Younossi Z, Tacke F, Arrese M, Chander Sharma B, Mostafa I, et al. Global perspectives on nonalcoholic fatty liver disease and non-alcoholic steatohepatitis. Hepatology 2019;69:2672–2682.
[3] Noncirrhotic nonalcoholic steatohepatitis with liver fibrosis: developing drugs for treatment guidance for industryU.S. Department of Health and Human Services Food and Drug Administration Center for Drug Evaluation and Research (CDER). 2018. https://www.fda.gov/media/119044/download.
[4] **Loomba R**, **Friedman SL**, **Shulman GI**. Mechanisms and disease consequences of nonalcoholic fatty liver disease. Cell 2021;184:2537–2564.
[5] Simon TG, Roelstraete B, Khalili H, Hagström H, Ludvigsson JF. Mortality in biopsy-confirmed nonalcoholic fatty liver disease: results from a nationwide cohort. Gut 2021;70:1375–1382.
[6] Angulo P, Kleiner DE, Dam-Larsen S, Adams LA, Bjornsson ES, Charatcharoenwitthaya P, et al. Liver fibrosis, but no other histologic features, is associated with long-term outcomes of patients with nonalcoholic fatty liver disease. Gastroenterology 2015;149:389–397.
[7] **Ekstedt M**, **Hagström H**, Nasr P, Fredrikson M, Stål P, Kechagias S, et al. Fibrosis stage is the strongest predictor for disease-specific mortality in NAFLD after up to 33 years of follow-up. Hepatology 2015;61:1547–1554.
[8] Sanyal AJ, Harrison SA, Ratziu V, Abdelmalek MF, Diehl AM, Caldwell S, et al. The natural history of advanced fibrosis due to nonalcoholic steatohepatitis: data from the simtuzumab trials. Hepatology 2019;70:1913–1927.
[9] Tsuchida T. Friedman SL Mechanisms of hepatic stellate cell activation. Nat Rev Gastroenterol Hepatol 2017;14:397–411.
[10] Brunt EM. Nonalcoholic fatty liver disease and the ongoing role of liver biopsy evaluation. Hepatol Commun 2017;1:370–378.
[11] Kleiner DE, Makhlouf HR. Histology of nonalcoholic fatty liver disease and nonalcoholic steatohepatitis in adults and children. Clin Liver Dis 2016;20:293–312.
[12] Burt AD, Lackner C, Tiniakos DG. Diagnosis and assessment of NAFLD: definitions and histopathological classification. Semin Liver Dis 2015;35:207–220.
[13] Reflection paper on regulatory requirements for the development of medicinal products for chronic non-infectious liver diseases (PBC, PSC, NASH). European Medicines Agency; 2018.
[14] Kleiner DE, Brunt EM, Van Natta M, Behling C, Contos MJ, Cummings OW, et al. Design and validation of a histological scoring system for nonalcoholic fatty liver disease. Hepatology 2005;41:1313–1321.
[15] Brunt EM, Janney CG, Di Bisceglie AM, Neuschwander-Tetri BA, Bacon BR. Nonalcoholic steatohepatitis: a proposal for grading and staging the histological lesions. Am J Gastroenterol 1999;94:2467–2474.
[16] Bedossa P, FLIP Consortium. Utility and appropriateness of the fatty liver inhibition of progression (FLIP) algorithm and steato-sis, activity, and fibrosis (SAF) score in the evaluation of biopsies of nonalcoholic fatty liver disease. Hepatology 2014;60:565–575.
[17] Standish RA, Cholongitas E, Dhillon A, Burroughs AK, Dhillon AP. An appraisal of the histopathological assessment of liver fibrosis. Gut 2006;55:569–578.
[18] Pai RK, Kleiner DE, Hart J, Adeyi QA, Andrew D, Clouston AD, et al. Standardising the interpretation of liver biopsies in non-alcoholic fatty liver disease clinical trials. Aliment Pharmacol Ther 2019;50:1100–1111.
[19] Gawrieh S, Knoedler DM, Saeian K, Wallace JR, Komorowski RA. Effects of interventions on intra- and interobserver agreement on interpretation of nonalcoholic fatty liver disease histology. Ann Diagn Pathol 2011;15:19–24.
[20] Davison BA, Harrison SA, Cotter G, Alkhouri N, Sanyal A, Edwards C, et al. Suboptimal reliability of liver biopsy evaluation has implications for randomized clinical trials. J Hepatol 2020;73:1322–1332.
[21] Kleiner DE, Brunt EM, Wilson LA, Behling C, Guy C, Contos M, et al. Association of histologic disease activity with progression of nonalcoholic fatty liver disease. JAMA Netw Open 2019;2(10):e1912565.
[22] Sun W, Chang S, Tai DC, Tan N, Xiao G, Tang H, et al. Nonlinear optical microscopy: use of second harmonic generation and two-photon microscopy for automated quantitative liver fibrosis studies. J Biomed Opt 2008;13:064010.
[23] Gailhouste L, Le Grand Y, Odin C, Guyader D, Turlin B, Ezan F, et al. Fibrillar collagen scoring by second harmonic microscopy: a new tool in the assessment of liver fibrosis. J Hepatol 2010;52:398–406.
[24] Xu S, Wang Y, Tai DCS, Wang S, Cheng CL, Peng Q, et al. qFibrosis: a fully-quantitative innovative method incorporating histological features to facilitate accurate fibrosis scoring in animal model and chronic hepatitis B patients. J Hepatol 2014;61:260–269.
[25] Liu F, Zhao JM, Rao HY, Yu WM, Zhang W, Theise ND, et al. Second harmonic generation reveals subtle fibrosis differences in adult and pediatric nonalcoholic fatty liver disease. Am J Clin Pathol 2017;148:502–512.
[26] Chang PE, Goh GBB, Leow WQ, Shen L, Lim KH, Tan CK. Second harmonic generation microscopy provides accurate auto-mated staging of liver fibrosis in patients with non-alcoholic fatty liver disease. PLoS One 2018;13:e0199166.
[27] Liu F, Goh GBB, Tiniakos D, Wee A, Leow WQ, Zhao JM, et al. qFIBS: an automated technique for quantitative evaluation of fibrosis, inflammation, ballooning, and steatosis in patients with nonalcoholic steatohepatitis. Hepatology 2020;71:1953–1966.
[28] Lucas KJ, Lopez P, Lawitz E, Sheikh A, Azenberg D, Hsia S, et al. Safety and efficacy of tropifexor in patients with fibrotic nonalcoholic steatohepatitis: 48-week results from Part C of the Phase 2 FLIGT-FXR study. Hepatology 2020;72(Suppl 1):101A. Abstract 139.
[29] Tully DC, Rucker PV, Chianelli D, Williams J, Vidal A, Alper PA, et al. Discovery of tropifexor (LJN452), a highly potent non-bile acid FXR agonist for the treatment of cholestatic liver diseases and nonalcoholic steatohepatitis (NASH). J Med Chem 2017;60:9960–9973.
[30] Hernandez ED, Zheng L, Kim Y, Fang B, Liu B, Valdez RA. Tropifexor-mediated abrogation of steatohepatitis and fibrosis is associated with the antioxidative gene expression profile in rodents. Hepatol Commun 2019;3:1085–1097.
[31] Goodman ZD, Becker Jr RL, Pockros PJ, Afdhal NH. Progression of fibrosis in advanced chronic hepatitis C: evaluation by morphometric image analysis. Hepatology 2007;45:886–894.
[32] Wang Y, Vincent R, Yang J, Asgharpour A, Liang X, Idowu MO, et al. Dual-photon microscopy-based quantitation of fibrosis-related parameters (q-FP) to model disease progression in steatohepatitis. Hepatology 2017;65:1891–1903.
[33] Brunt EM, Clouston AD, Goodman Z, Guy C, Kleiner DE, Lackner C, et al. The complexity of ballooned hepatocyte feature recognition: defining a training atlas for imaging-based artificial intelligence in NAFLD. J Hepatol 2022;76(5):1030–1041. https://doi.org/10.1016/j.jhep.2022.01.011.
[34] Sun Y, Zhou J, Wang L, Wu X, Chen Y, Piao H, et al. New classification of liver biopsy assessment for fibrosis in chronic hepatitis B patients before and after treatment. Hepatology 2017;65:1438–1450.

[35] Kleiner DE. On beyond staging and grading: liver biopsy evaluation in a posttreatment world. Hepatology 2017;65:1432–1434. https://doi.org/10.1002/hep.29111.
[36] Harrison SA, Tai D, Ren Y, Taub Bashir MR. Steatosis and fibrosis measured as continuous variables on paired, serial liver biopsies in the resmetirom (MGL-3196) 36-week phase 2 NASH study. In: AASLD; 2019. Abstract #2133.
[37] Decaris ML, Li KW, Emson CL, Gatmaitan M, Liu S, Wang Y, et al. Identifying nonalcoholic fatty liver disease patients with active fibrosis by measuring extracellular matrix remodeling rates in tissue and blood. Hepatology 2017;65:78–88.
[38] Boyle M, Tiniakos D, Schattenberg JM, Ratziu V, Bugianessi E, et al. Performance of the PRO-C3 collagen neo-epitope biomarker in non-alcoholic fatty liver disease. JHEP Rep 2019;1:188–198.
[39] Vali Y, Lee J, Boursier J, Spijker R, Löffler J, Verheij J, et al. Enhanced liver fibrosis test for the non-invasive diagnosis of fibrosis in patients with NAFLD: a systematic review and meta-analysis. J Hepatol 2020;73:252–262.
[40] Sun Y, Zhou J, Wu X, Chen Y, Piao H, Lu L, et al. Quantitative assessment of liver fibrosis (qFibrosis) reveals precise outcomes in Ishak 'stable' patients on anti-HBV therapy. Sci Rep 2018;8:2989.
[41] Wang Y, Wong GL, He FP, Sun J, Chan AW, Yang J, et al. Quantifying and monitoring fibrosis in non-alcoholic fatty liver disease using dual-photon microscopy. Gut 2020;69:1116–1126.
[42] Soon G, Wee A. Updates in the quantitative assessment of liver fibrosis for nonalcoholic fatty liver disease: histological perspective. Clin Mol Hepatol 2021;27:44–57.
[43] Forlano R, Mullish BH, Giannakeas N, Maurice JB, Angkathunyakul N, Lloyd J, et al. High-throughput, machine learning-based quantification of steatosis, inflammation, ballooning, and fibrosis in biopsies from patients with nonalcoholic fatty liver disease. Clin Gastroenterol Hepatol 2020;18:2081–2090.e9.
[44] Gawrieh S, Sethunath D, Cummings OW, Kleiner DE, Vuppalanchi R, Chalasani N, et al. Automated quantification and architectural pattern detection of hepatic fibrosis in NAFLD. Ann Diagn Pathol 2020;47:151518.
[45] De Rudder M, Bouzin C, Nachit M, Louvegny H, Velde GV, Julé Y, et al. Automated computerized image analysis for the user-independent evaluation of disease severity in preclinical models of NAFLD/NASH. Lab Invest 2020;100:147–160.
[46] Briand F, Maupoint J, Brousseau E, Breyner N, Bouchet M, Costard C, et al. Elafibranor improves diet-induced nonalcoholic steatohepatitis associated with heart failure with preserved ejection fraction in Golden Syrian hamsters. Metabolism 2021;117:154707.
[47] Taylor-Weiner A, Pokkalla H, Han L, Jia C, Huss R, Chung C, et al. A machine learning approach enables quantitative measurement of liver histology and disease monitoring in NASH. Hepatology 2021;74:133–147.
[48] Loomba R, Noureddin M, Kowdley KV, Kohli A, Sheikh A, Neff G, et al. Combination therapies including cilofexor and firsocostat for bridging fibrosis and cirrhosis attributable to NASH. Hepatology 2021;73:625–643.
[49] Paradis V, Quaglia A. Digital pathology, what is the future? J Hepatol 2019;70:1016–1018.
[50] Saillard C, Schmauch B, Laifa O, Moarii M, Toldo S, Zaslavskiy M, et al. Predicting survival after hepatocellular carcinoma resection using deep learning on histological slides. Hepatology 2020;72:2000–2013.
[51] Wanless I. Quantitative SHG-microscopy: unraveling the nano-architecture of the cirrhotic liver. Clin Res Hepatol Gastroenterol 2020;44:1–3.
[52] Azam AS, Miligy IM, Kimani P, Maqbool H, Hewitt K, Rajpoot NM, et al. Diagnostic concordance and discordance in digital pathology: a systematic review and meta-analysis. J Clin Pathol 2021;74:448–455.